Characterization of lithium alkyl carbonates by X-ray photoelectron spectroscopy: Experimental and theoretical study

Rémi Dedryvère, L. Gireaud, S. Grugeon, S. Laruelle, J.-M. Tarascon, Danielle Gonbeau

Characterization of Lithium Alkyl Carbonates $ROCO_2Li$ by X-ray Photoelectron Spectroscopy (XPS) : Experimental and Theoretical Study

R. Dedryvère [a,*], L. Gireaud [b], S. Grugeon [b], S. Laruelle [b], J-M. Tarascon [b], D. Gonbeau [a]

[a] LCTPCM, Université de Pau, Hélioparc Pau Pyrénées, 2 av. Pierre Angot, 64053 Pau cedex 9, France

[b] LRCS, Université de Picardie Jules Verne, 33 rue Saint-Leu, 80039 Amiens, France

Abstract

Lithium alkyl carbonates $ROCO_2Li$ result from the reductive decomposition of dialkyl carbonates, which are the organic solvents used in the electrolytes of common lithium-ion batteries. They play a crucial role on the formation of surface layers at the electrode/electrolyte interfaces. In this work, we first report on the XPS characterization of synthesized lithium methyl and ethyl carbonates. By means of Hartree-Fock ab initio calculations, we interpret and simulate the valence spectra of both samples, as well as several other Li alkyl carbonates involved in Li-ion batteries. We show that Li alkyl carbonates can be identified at electrode's surfaces by a combined analysis of XPS core peaks and valence spectra.

Keywords : Lithium alkyl carbonates, XPS, valence spectra, lithium-ion batteries, ab initio, Hartree-Fock, simulation

* corresponding author (remi.dedryvere@univ-pau.fr)

INTRODUCTION

Rechargeable Li-ion batteries are the key component of today's portable electronics, and are also standing as serious candidates over Ni-MeH batteries for the next generation of hybrid electric vehicles. This growing worldwide need requires an enhanced understanding of the science underlying Li-ion battery technology to improve performances of this type of power sources [1,2]. Many research trends have been aimed at optimizing components of the operating systems, consisting of a graphitic carbon anode, a layered transition metal oxide cathode such as $LiCoO_2$, and a nonaqueous organic electrolyte based on alkyl carbonate solvents such as dimethyl carbonate (DMC), ethylene carbonate (EC) or propylene carbonate (PC). It is common knowledge that cycle life and stability of Li-ion batteries are very dependent on the formation of an organic/inorganic layer at the graphite anode/electrolyte interface, usually known as the solid electrolyte interphase (SEI) layer [3,4,5,6]. While it is generally admitted that the SEI layer originates from the reductive decomposition of the solvents and salt during the first charge/discharge cycle of the battery, its mechanism of formation on Li or carbonaceous materials as well as its composition and nature are still subject to numerous controversial discussions, and still monopolize a lot of research efforts. Interestingly, independently of the carbonated solvents, the same prevailing species such as Li_2CO_3 and lithium alkyl carbonates ($ROCO_2Li$) are often revealed by infrared spectrometry as the main SEI components [6,7,8,9].

Recently, in a study about the electrochemical reduction of 3d-metal oxides (MO_x) in lithium cells, we displayed the growth and disappearance of an organic/inorganic layer at the surface of the metal oxide particles upon cycling, which entails a temperature-driven capacity enhancement and long-term cyclability of the cells [10,11,12,13]. Such an effect seems to be

not specific to metal oxides, since it was also observed for nitrides such as Cu_3N [14]. Moreover, we also observed the formation of the same kind of organic/inorganic layer at the surface of stainless-steel electrodes. Using characterization techniques such as Fourier-Transform Infrared Spectroscopy (FTIR) or High Resolution Mass Spectrometry (HRMS), we could detect the presence of various compounds in these layers, including lithium alkyl carbonates [13]. Thus, the formation of lithium alkyl carbonates seems to be a recurrent process when carbonated solvents are used in the electrolyte.

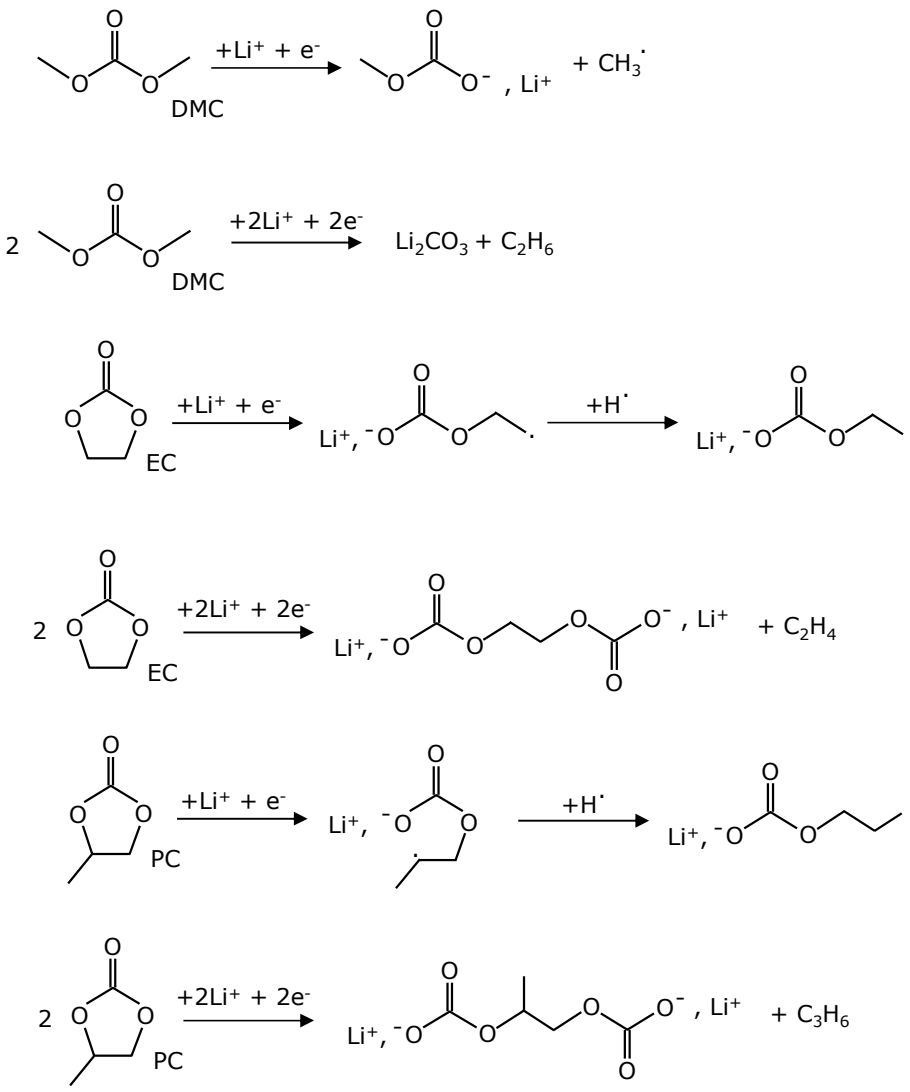

Figure 1 : Mechanisms commonly proposed to explain the formation of Li alkyl carbonates in Li-ion batteries by reduction of the organic solvents.

Numerous mechanisms have been proposed to explain their formation by reduction of the solvents [15,16]. In Figure 1 are reported the most often cited reduction mechanisms of DMC, EC and PC leading to the formation of Li methyl carbonate ($MeOCO_2Li$), Li ethyl carbonate ($EtOCO_2Li$), Li propyl carbonate ($PrOCO_2Li$), Li ethylene dicarbonate $(-CH_2OCO_2Li)_2$, Li propylene dicarbonate ($LiO_2CO\text{-}CH(CH_3)CH_2\text{-}OCO_2Li$), and Li_2CO_3. The most common characterization technique used to analyze electrode/electrolyte interfaces and identify Li alkyl carbonates is FTIR, which enables the identification of functional groups of the various species. Since the early work of Behrendt et al. [17], Li alkyl carbonates have been generally characterized by this technique. However, the accurate distinction of Li alkyl carbonates salts in complex mixtures with Li_2CO_3, as often observed at the electrode/electrolyte interface in presence of these carbonated solvents, still remains hazardous because of their spectral similitude in the 1200-1700cm^{-1} wavenumber range. Finally, only Li methyl carbonate is clearly distinguishable thanks to both 1196 and 936 cm^{-1} wavelengths.

X-ray Photoelectron Spectroscopy (XPS) is also commonly used to characterize electrodes surfaces. However, efficient identification of Li alkyl carbonates is difficult due to the lack of experimental reference data and extensive studies concerning these compounds. Particularly, to our knowledge no experimental work was reported to show if it is possible to discriminate $ROCO_2Li$ species from Li_2CO_3 by XPS.

In this work, we will report on the XPS characterization of synthesized $MeOCO_2Li$ and $EtOCO_2Li$ by recording their C 1s, O 1s and Li 1s core peaks and valence spectra. Then, we will propose a careful analysis of their valence spectra with the help of ab initio Hartree-Fock calculations, which allow us to simulate them. We will then calculate valence spectra of other Li alkyl carbonates, namely $PrOCO_2Li$, $(-CH_2OCO_2Li)_2$ and $LiO_2CO\text{-}CH(CH_3)CH_2\text{-}OCO_2Li$.

Our aim is to show that the different Li alkyl carbonates are easily distinguishable by a coupled core and valence XPS analysis. Finally, the results of this study will be used to characterize the layers forming at the surface of stainless-steel cathodes in lithium cells.

EXPERIMENTAL

Sample preparation

1. Lithium alkyl carbonates

Lithium methoxide and ethoxide were purchased from Sigma-Aldrich. Extra-dry methanol and ethanol were purchased from Carlo Erba.

1.1. Lithium methyl carbonate :

Lithium methoxide (300 mg) was dissolved in 30 mL absolute methanol. After 15 min of vigorous stirring under argon, the solution was bubbled with CO_2 at room temperature for 3 hours. The solvent was then evaporated under reduced pressure with a rotary evaporator, and the resulting slurry was dried under vacuum to give a white crystal that was kept under argon between -5°C and 0°C [9].

1.2. Lithium ethyl carbonate:

Lithium ethyl carbonate was synthesized using a similar procedure as above. 500 mg of lithium ethoxide were dissolved into 50 mL of absolute ethanol to produce 700 mg of white lithium ethyl carbonate after both evaporation and drying steps.

After lithium alkyl carbonate salts synthesis, their purities have been proved by means of infrared (ATR), Nuclear Magnetic Resonance (NMR) and Electrospray Mass Spectrometry

in positive mode (ESI-MS).

2. Electrochemical experiments

Electrochemical coin cells were made using a 16 mm diameter treated stainless steel disc as the positive electrode, Li metal as the negative electrode and an electrolyte-saturated Whatman borosilicate glass fiber sheet as the separator. The electrolyte used was a 1M $LiPF_6$ solution in 1:1 weight ratio of dimethyl carbonate (DMC) and ethylene carbonate (EC). The cells were assembled in argon dry-box, and then placed into an oven prior to being cycled at 55°C by means of a Macpile system (Biologic S.A., Claix, France) performing in a galvanostatic mode. The cells were cycled between 0.02-3V with a 0.16 mA/cm^2 current density. The stainless steel disc was carefully separated from the rest of the battery components, washed with acetonitrile to remove the electrolyte, and dried prior to being packed into a hermetically sealed aluminium plastic bag for transportation. The side of the stainless steel disc facing the electrolyte was analyzed by XPS.

XPS measurements

To prevent any sample from moisture/air exposure on the analysis site, the XPS spectrometer was directly connected through a transfer chamber to a nitrogen dry-box. The samples were removed from their packaging within the dry-box and placed onto the sample holder without any contamination. Li_2CO_3 and lithium alkylcarbonates were also grinded in an agate mortar before being placed onto the sample holder. XPS measurements were carried out with a Kratos Axis Ultra spectrometer using a focused monochromatized Al Kα radiation ($h\nu$ = 1486.6 eV). The spectrometer was calibrated using the photoemission line Ag $3d_{5/2}$ (binding energy 368.3 eV). For the Ag $3d_{5/2}$ line the full width at half maximum (FWHM)

was 0.61 eV under the recording conditions. Core peaks and valence spectra were recorded with 20 eV constant pass energy. The analyzed area of the samples was 300×700 μm^2. Charge neutralization was used for all measurements, the pressure in the analysis chamber was about 5.10^{-7} Pa, and the temperature of the samples was regulated at -140°C to avoid a possible degradation due to the X-ray beam. Control spectra were recorded at the beginning and at the end of each experiment to check the non-degradation of the samples. The binding energy (BE) scale was calibrated from the carbon contamination using the C 1s peak at 285.0 eV. Core peaks were analyzed using a non-linear Shirley-type background [18], and peak positions and areas were obtained by a weighed least-square fitting of model curves (70% Gaussian, 30% Lorentzian) to the experimental data. Quantification was performed on the basis of Scofield's relative sensitivity factors [19]. For a more accurate analysis of valence spectra of electrochemically prepared samples, simulated spectra obtained from a weighed fitting of reference compounds spectra (LiF, Li_2CO_3, $MeOCO_2Li$) to the experimental curve were reported (This concerns only Fig. 9 and 10. The other simulated spectra have been calculated by the theoretical method described below).

COMPUTATIONAL DETAILS

Calculations were carried out to determine the monoelectronic energy levels of the various carbonate compounds in order to interpret and simulate their valence XP spectra in the Koopman's theorem approximation. These calculations were performed with the GAUSSIAN 98 program [20] using the restricted Hartree-Fock self-consistent method and the standard 6-311G* basis set. The geometrical parameters were optimized by a gradient method.

The intensities of valence XP spectra were estimated using the Gelius intensity model [21,22], which is based on the assumption that the cross-section of a molecular orbital (MO) is determined only by the cross-sections of the corresponding atomic orbitals (AO). According to this model, the intensity of the j^{th} MO is given by the following equation :

$$I_j \approx (2 + \frac{\beta_j}{2}) \sum_{i\ AO} P_{j,i}\ \sigma_i \qquad (1)$$

where : i refers to the i^{th} AO

β_j is an asymmetry factor

$P_{j,i}$ are factors describing the weight of the contribution of the i^{th} AO to the MO

σ_i is the atomic photoionization cross-section relating to the i^{th} AO

For each MO, the weighted sum is extended over all the valence AO, namely O 2s, O 2p, C 2s, C 2p, Li 2s and H 1s. The corresponding atomic photoionization cross-sections are 0.14 , 0.0193 , 0.0477 , 0.0015 , 0.0008 and 0.0 respectively [19].

Simulated valence XP spectra were constructed from the monoelectronic energy levels ε_j and the intensities I_j calculated for each MO. They consist of a series of peaks centered at the monoelectronic energies ε_j. In order to obtain a simulation closer to the experiment, each peak was represented by a functional shape made of a combination of Gaussian and Lorentzian profiles (70% Gaussian, 30% Lorentzian) having the same width (1.6 eV) to simulate the experimental resolution of the spectrometer. As usually in this kind of simulation, the energy scale of the so-obtained spectra was shifted to account for relaxation and correlation effects as well as differences in reference levels. Finally, the best fit with the

experimental spectrum is obtained after a linear contraction of the BE scale.

RESULTS AND DISCUSSIONS

1. XPS characterization of $MeOCO_2Li$ and $EtOCO_2Li$

Figure 2 shows XPS C 1s, O 1s and Li 1s core peaks of : *a)* Li_2CO_3 (as reference compound), *b)* $MeOCO_2Li$ and *c)* $EtOCO_2Li$. All spectra are reported without any fitting of the peaks for more clarity. No extra element could be detected on survey spectra.

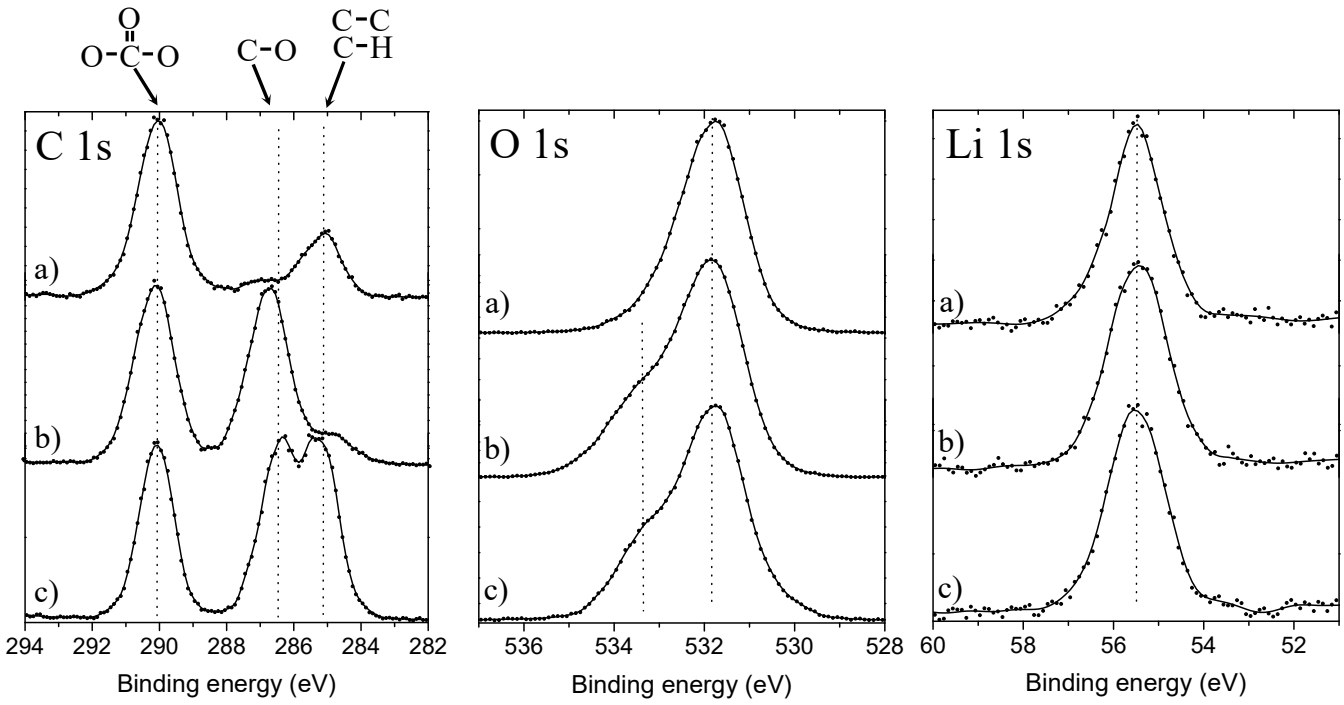

Figure 2 : Experimental C 1s, O 1s and Li 1s core peaks of : **a)** Li_2CO_3, **b)** $MeOCO_2Li$ and **c)** $EtOCO_2Li$.

C 1s core peaks : As expected, the spectrum of Li_2CO_3 (2 a) shows a main peak at 290.1eV assigned to carbon atoms in a three-oxygen environment (CO_3-like). The other peaks are due to surface contamination. Particularly, the peak at 285.0 eV corresponds to hydrocarbon contamination always observed in variable quantities at the surface.

The spectrum of $MeOCO_2Li$ (2 b) shows two main peaks of equal intensity at 286.7 and 290.1 eV. This is in good agreement with the formula of this compound including two kinds of carbon atoms : CO-like and CO_3-like, respectively. A weak hydrocarbon contamination can be also detected at 285.0 eV.

The spectrum of $EtOCO_2Li$ (2 c) shows three peaks of equal intensity at 285.3, 286.4 and 290.1 eV. This is in good agreement with the $CH_3CH_2OCO_2Li$ formula. The first peak (285.3 eV) corresponds to the carbon atom bound only to C or H atoms, and both peaks at 286.4 and 290.1 eV correspond to CO-like and CO_3-like carbons, respectively.

It is worth noting that there is no significant BE shift of the CO_3-like peak from Li_2CO_3 to $MeOCO_2Li$ and $EtOCO_2Li$. Indeed, one could expect a small increase of the BE due the replacement of one lithium in the formula by an alkyl group. For example, our measurements made in the same conditions on diethyl carbonate $C_2H_5OCO_2C_2H_5$ (DEC, frozen liquid at -140°C) showed a CO_3-like peak at 290.5 eV. But we can see from Fig. 2 that there is no BE difference for this peak between Li_2CO_3, $MeOCO_2Li$ and $EtOCO_2Li$.

O 1s core peaks : The O 1s spectrum of Li_2CO_3 (2 a) consists of one peak with a maximum at 531.8 eV. The shape of this peak is slightly asymmetric : this can be explained by the crystallographic structure of Li_2CO_3 [23], in which two oxygen atoms have an identical environment with one C at 1.27 Å and three Li at 1.96-2.00 Å, and the third oxygen has a different environment with one C at 1.28 Å and two Li at 1.96 Å. Thus, the oxygen having

only two Li in its neighbourhood is expected at a higher BE in the O 1s peak than both oxygens having three Li neighbours.

The O 1s spectra of $MeOCO_2Li$ and $EtOCO_2Li$ (2 b,c) also show an asymmetrical profile, with a maximum at 531.8 eV. The asymmetry is here much greater since a shoulder can be easily distinguishable at 533.3 eV in each case. This can be explained by the local environment of oxygen atoms. Although to our knowledge the crystallographic structures of $MeOCO_2Li$ and $EtOCO_2Li$ have not been reported, it is clear that oxygen atoms have very different environments : two of them are bound to one C and have Li^+ neighbours, while the third one is bound to two carbon atoms.

Li 1s core peaks : All samples show very similar Li 1s spectra, which consist of a symmetrical peak at 55.5 eV.

Experimental valence spectra :

Figure 3 shows the experimental valence spectra of the same samples : *a)* Li_2CO_3, *b)* $MeOCO_2Li$ and *c)* $EtOCO_2Li$. The spectrum of Li_2CO_3 consists of a large massif at 22-31 eV (with a narrow maximum at 24.3 eV, a shoulder at 26.3 and a peak at 28.9 eV), of two narrow peaks at 12.9 and 10.8 eV, and of a massif at 4-8 eV with a maximum at 6.0 eV. The assignment of each component of this spectrum will be detailed below.

The spectrum of $MeOCO_2Li$ resembles that of Li_2CO_3, except two main differences : *i)* the decrease of the narrow peak at 24.3 eV which is replaced by a shoulder, and *ii)* the appearance of an extra peak at 17.6 eV. The spectrum of $EtOCO_2Li$ (3 c) is very close to that of $MeOCO_2Li$. The main difference consists in the appearance of two extra peaks at 15.4 and 18.8 eV instead of one. An other small difference is the appearance of a small peak at 8.7 eV.

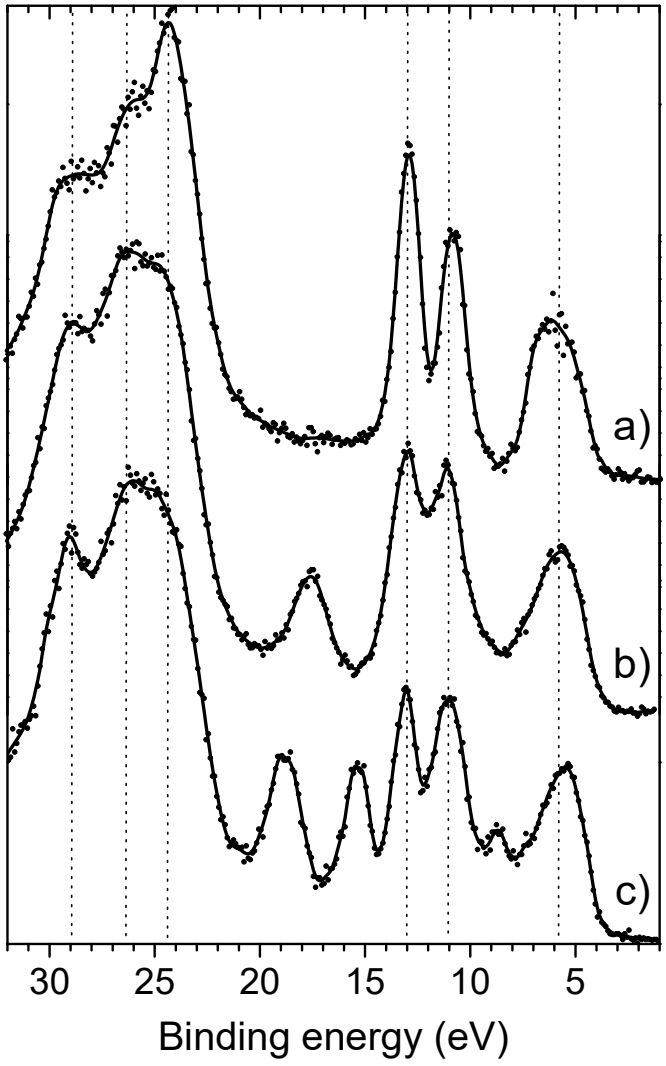

Figure 3 : Experimental valence spectra of : **a)** Li_2CO_3, **b)** $MeOCO_2Li$ and **c)** $EtOCO_2Li$.

2. Calculations and simulated valence spectra

The aim of this approach is the interpretation and the prediction of Li alkyl carbonates valence spectra. Due to the lack of experimental structural data on these compounds (except

Li_2CO_3) the optimization of geometrical parameters was necessary. The results obtained for bond distances and angles are reported in Figure 4.

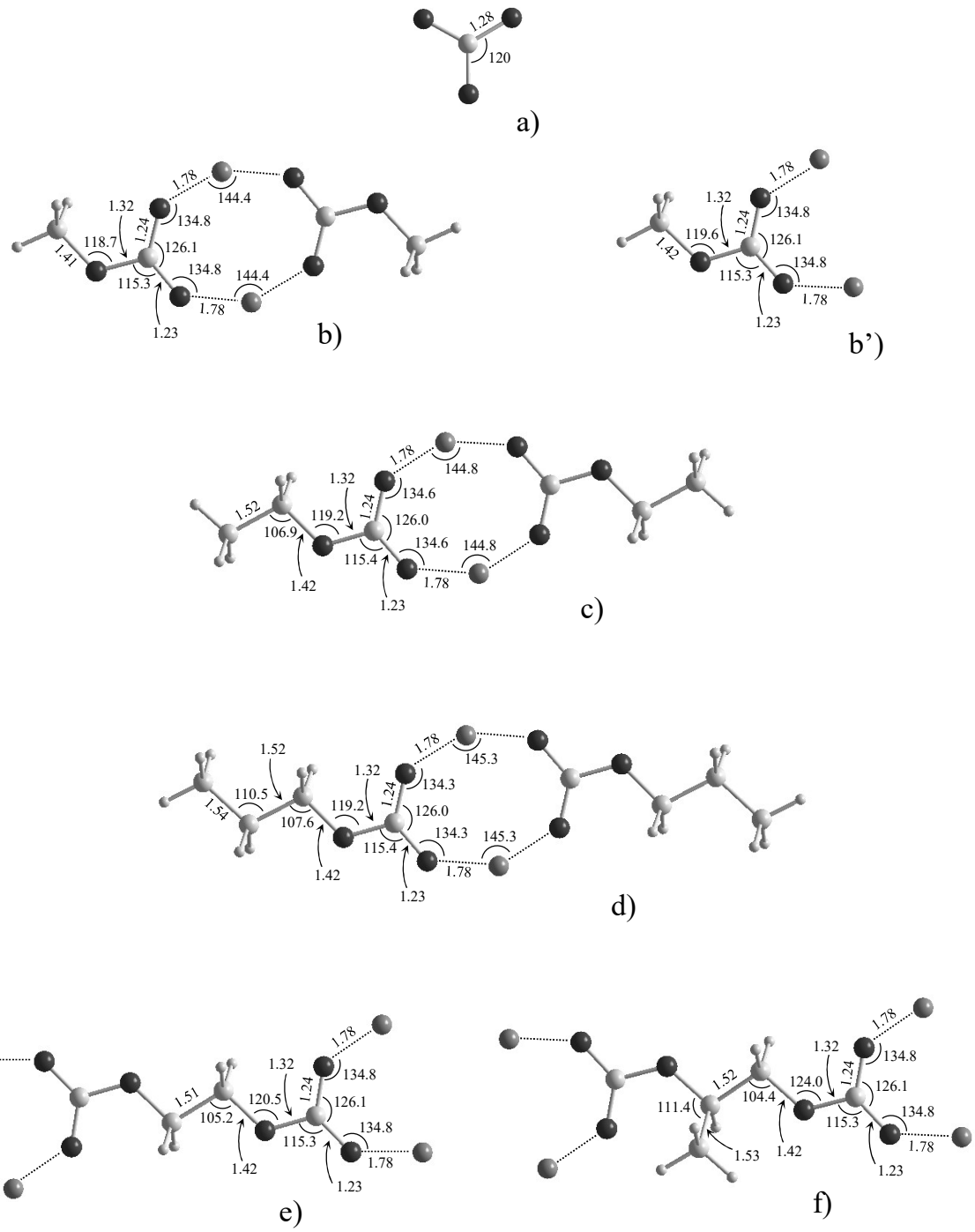

Figure 4 : Optimized structures of : **a)** Li_2CO_3 (simple CO_3^{2-} anion), **b)** $MeOCO_2Li$ (dimer), **b')** $MeOCO_2Li_2^+$ (positive ion), **c)** $EtOCO_2Li$ (dimer), **d)** $PrOCO_2Li$ (dimer), **e)** $(-CH_2OCO_2Li_2)_2^{2+}$ and **f)** $Li_2O_2CO\text{-}CH(CH_3)CH_2\text{-}OCO_2Li_2^{2+}$. Dark grey balls stand for O atoms, light grey ones for C, medium grey ones for Li and small ones for H atoms.

For Li_2CO_3, two models were considered : a simple CO_3^{2-} ion with a planar geometry and O-C-O angles of 120° (fig. 4 a), and a $Li_8CO_3^{6+}$ cluster with atomic positions taken from the crystallographic structure. As very similar results were obtained, only the CO_3^{2-} model will be considered in the following. This can be explained by the very low contribution of lithium AO to the valence MO.

For the Li alkyl carbonates $MeOCO_2Li$, $EtOCO_2Li$ and $PrOCO_2Li$, neutral monomer structures were not satisfactory to interpret and simulate the valence spectra. Therefore, dimer structures $(ROCO_2Li)_2$ were considered (fig. 4 b,c,d). Lengths and angles were optimized with the molecule being forced to fit the C_{2h} geometry. Note that this kind of dimer model structures was already successfully taken for Hartree-Fock and Density Functional Theory (DFT) calculations of the vibrational frequencies of infrared spectra of Li alkyl carbonates [24,25]. In our study, monomer structures of $ROCO_2Li_2^+$ ions also gave good results, as it will be shown below. The ion monomer structure $MeOCO_2Li_2^+$ is illustrated in fig. 4 b').

For Li ethylene and propylene dicarbonates $(-CH_2OCO_2)_2Li_2$ and $LiO_2CO-CH(CH_3)CH_2-OCO_2Li$ (fig. 4 e and f), the difficulty to build dimers led us to only consider monomer positive ions $(-CH_2OCO_2Li_2)_2^{2+}$ and $Li_2O_2CO-CH(CH_3)CH_2-OCO_2Li_2^{2+}$.

Using the simple CO_3^{2-} model ion, the computational method described before allowed us to assign the different components of the valence spectrum of Li_2CO_3. Figure 5 shows the experimental spectrum, the calculated spectrum (vertical bars), together with a diagram of the MO corresponding to the different monoelectronic energy levels. Only the dominant characters of the MO have been illustrated. Calculations results allowed us to assign the large massif at 22-31 eV to the photoionization of three MO of dominant O 2s character. Note that the very simple chosen model doesn't allow us to distinguish the narrow peak at 24.3 eV from the shoulder at 26.3 eV. Both narrow peaks at 10.8 and 12.9 eV can be assigned to the

photoionization of MO with dominant O 2p, C 2s and C 2p character. Thus, these two peaks are representative of C-O bonds in Li_2CO_3. Finally, the massif at 4-8 eV can be assigned to the photoionization of non-bonding MO of dominant O 2p character (lone pairs).

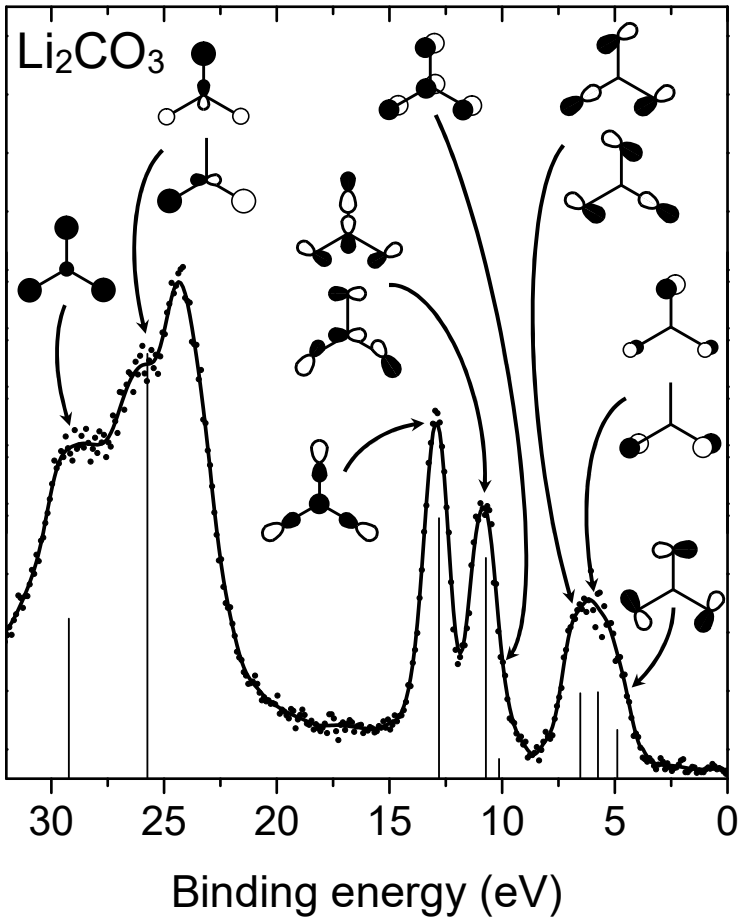

Figure 5 : Experimental and calculated (vertical bars) valence spectra of Li_2CO_3, with MO corresponding to the different energy levels.

Simulated spectra can be generated as defined in the computational details section. Figure 6 shows experimental and simulated spectra of Li_2CO_3, $MeOCO_2Li$ and $EtOCO_2Li$ corresponding to optimized geometries given in fig. 4. On the figure have been also illustrated

the MO corresponding to valence peaks characteristic of $MeOCO_2Li$ and $EtOCO_2Li$ in the 14-21 eV energy region. The calculations results showed that the additional peaks appearing in this region are due to the photoionization of MO with dominant C 2s character resulting from the presence of additional carbon atoms in the molecule.

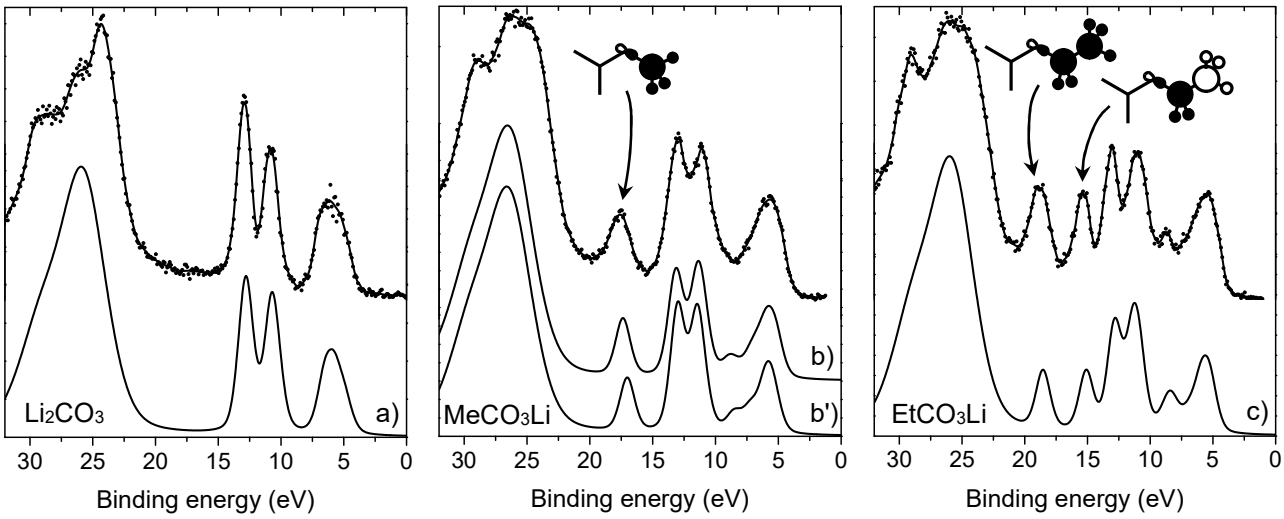

Figure 6 : Experimental and calculated valence spectra of Li_2CO_3, $MeOCO_2Li$ and $EtOCO_2Li$. **a)**, **b)**, **b')** and **c**) refer to the geometries of fig. 4. MO of dominant C 2s character in the 14-21 eV energy region have been represented.

For $MeOCO_2Li$, the peak at 17.6 eV results from one MO. For $EtOCO_2Li$, both peaks at 15.4 and 18.8 eV ensue from two MO, the first one being anti-bonding and the second one bonding, respectively. For $MeOCO_2Li$, both geometry choices give satisfactory results. The dimer structure b) is closer to the experiment, but the monomer $CH_3OCO_2Li_2^+$ ion b') is also suitable to simulate the valence spectrum.

For $EtOCO_2Li$, the calculation method is also efficient to interpret the small peak observed at about 8 eV. According to the calculations results, this peak can be assigned to bonding MO of dominant O 2p and C 2p character, which are representative of C-C and C-O

bonds existing in $ROCO_2Li$ and not in Li_2CO_3. Note that a very small peak at about 8 eV is also observed in the simulated spectrum of $MeOCO_2Li$, while this peak is hardly detectable in the experimental spectrum.

The overall conclusion of this analysis is that the calculation method and the geometry models chosen here are quite efficient to interpret and simulate valence spectra of these Li alkyl carbonates.

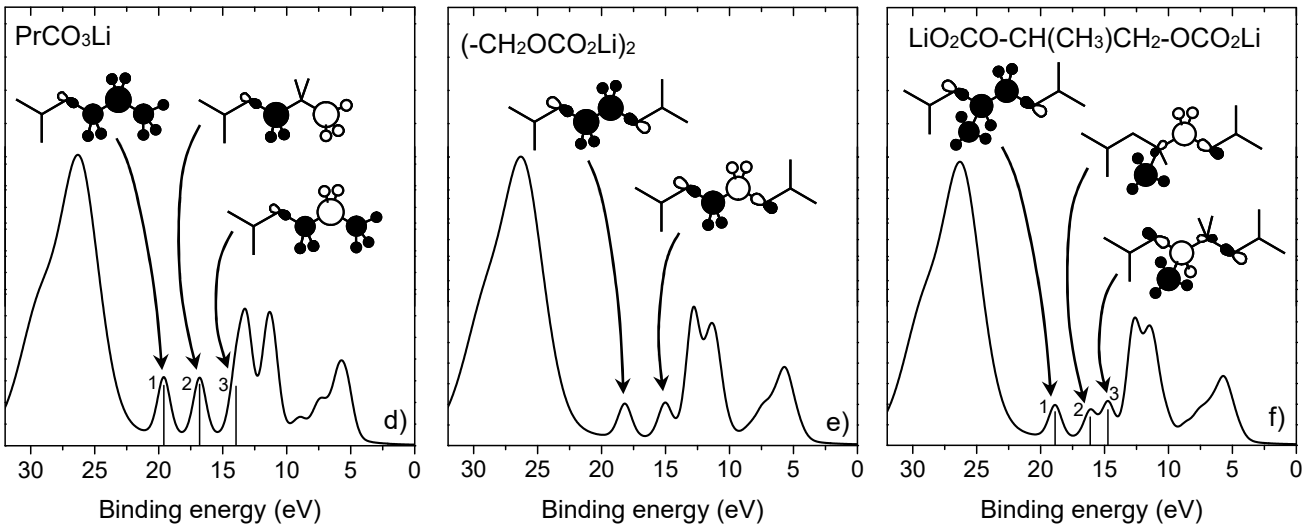

Figure 7 : **C**alculated valence spectra of $PrOCO_2Li$, $(-CH_2OCO_2Li)_2$ and $LiO_2CO\text{-}CH(CH_3)CH_2\text{-}OCO_2Li$. **d)**, **e)** and **f)** refer to the geometries of figure 4. MO of dominant C 2s character in the 14-21 eV energy region have been represented.

In the following, we carried out the same kind of analysis with three other Li alkyl carbonates, namely $PrOCO_2Li$, $(-CH_2OCO_2)_2Li_2$ and $LiO_2CO\text{-}CH(CH_3)CH_2\text{-}OCO_2Li$. For these samples, up to now experimental XPS characterization could not be performed because of the difficulty to synthesize pure samples. Therefore, using the same theoretical method as before, we will present here only calculated spectra. Figure 7 shows the calculated spectra of

these compounds, corresponding to the geometries given in figure 4. The diagrams of MO corresponding to peaks in the 14-21 eV region have been reported.

For $PrOCO_2Li$, as we can see in the figure, the presence of three additional carbon atoms in the molecule as compared to Li_2CO_3 results in the appearance of three additional peaks corresponding to three MO of dominant C 2s bonding and anti-bonding character. These results are consistent with the previous work of Pireaux et al. [26] showing the evolution of XP valence spectra of linear alkanes C_nH_{2n+2} with increasing *n*, and displaying the presence of *n* peaks due to *n* MO of dominant C 2s character. In $PrOCO_2Li$, according to our calculations, the lowest BE peak (peak n°3) should be superposed on the narrow peak observed at 12.9-13.0 eV, and thus should modify the shape of the 10-13 eV massif. However, the presence of two well resolved peaks between 15 and 21 eV is definite.

Lithium ethylene dicarbonate and lithium propylene dicarbonate are of great importance in the Li-ion battery field since they are very often cited as the main degradation products present at the electrode/electrolyte interface, when EC or PC is used as solvent respectively [8]. The simulated spectrum of $(-CH_2OCO_2)_2Li_2$ shown in Figure 7 exhibits two peaks in the 14-21 eV region that can be assigned to two MO of dominant C 2s bonding and anti-bonding character. As a result, the valence spectrum of this sample could be rather close to that of $EtOCO_2Li$. However, small differences are expected concerning the intensities because the number of oxygen atoms in $(-CH_2OCO_2)_2Li_2$ is greater than in $EtOCO_2Li$. Moreover, both compounds are expected to be well distinguishable by their C 1s core spectra, since the spectrum of $(-CH_2OCO_2)_2Li_2$ should consist of two peaks of equal intensity at 290 and 286-287 eV assigned to CO_3 and CO environments of carbon atoms, while the spectrum of $EtOCO_2Li$ consists of three peaks of equal intensity, as detailed before.

The simulated spectrum of $LiO_2CO\text{-}CH(CH_3)CH_2\text{-}OCO_2Li$ shown in Figure 7 exhibits three peaks in the 14-21 eV region that can be assigned to three MO of dominant C 2s bonding and anti-bonding character. This way, the valence spectrum of this sample should be close to that of $PrOCO_2Li$. However, a difference concerning the peak positions allows to distinguish both spectra. According to our calculations, peak n°3 should not be superposed on the narrow peak at 12.9-13.0 eV. This can be explained by the lower anti-bonding character of MO n°3 in $LiO_2CO\text{-}CH(CH_3)CH_2\text{-}OCO_2Li$ than in $PrOCO_2Li$.

As a conclusion, we showed in this part that the common Li alkyl carbonates can be easily identified by a combined analysis of their XPS core peaks and valence spectra.

3. Application to XPS study of electrode/electrolyte interfaces

In the following, we propose a first example of application of this dual experimental and theoretical approach to characterize surface layers forming at the electrode/electrolyte interface by a detailed interpretation of their XP valence spectra. The samples studied here are stainless-steel cathodes removed from electrochemical cells using metallic lithium as anode and a liquid electrolyte consisting of $LiPF_6$ in an EC/DMC solution.

Figure 8 shows XPS C 1s core peaks of cathodes removed from electrochemical cells after : *a)* a first discharge down to 0.02 V and *b)* after 500 cycles of discharge/charge, and washed by acetonitrile to remove the excess of electrolyte from the surface. The C 1s spectrum of sample a) consists of three peaks at 290.1, 286.8 and 285.0 eV that can be assigned to CO_3, CO and C-C/C-H carbon environments respectively. The large peak at 290.1 eV and the small peak at 286.8 eV allow us to suppose that Li_2CO_3 is the major carbon-

containing species at the surface. The peak at 286.8 eV can be either attributed to a small amount of Li alkyl carbonate or to other species contaminating the surface. The peak at 285.0 eV is assigned to contaminating hydrocarbon.

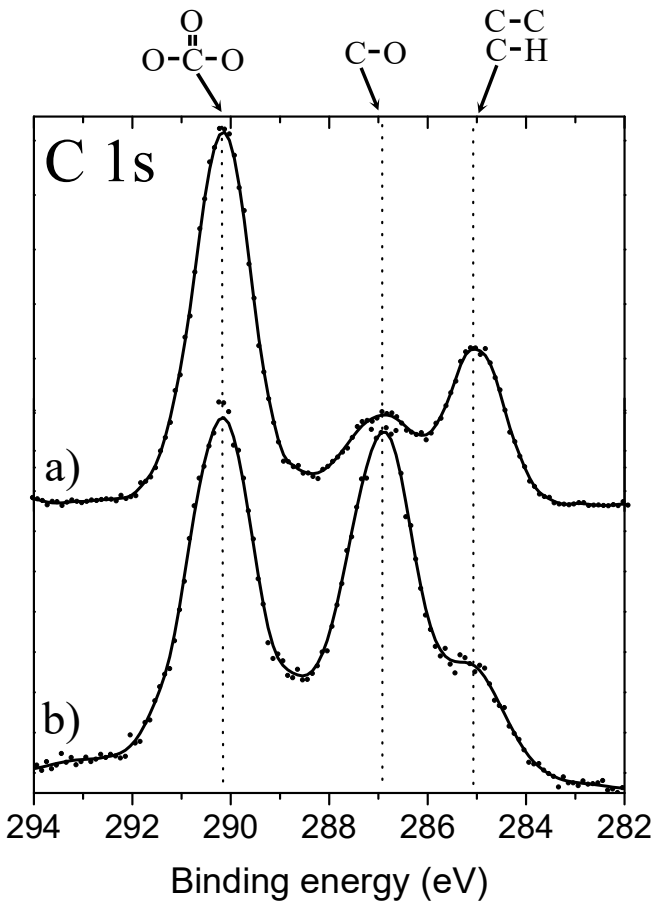

Figure 8 : Experimental C 1s core peaks of the surface layers of stainless-steel electrodes after : **a)** first discharge, **b)** 500 cycles.

The C 1s spectrum of sample b) obtained after 500 cycles exhibits a very different shape. Besides the small hydrocarbon contamination at 285.0 eV, it consists of two peaks of equal intensity at 290.1 and 286.8 eV, which is exactly the expected spectrum for $MeOCO_2Li$ but also for Li ethylene dicarbonate $(-CH_2OCO_2)_2Li_2$. Moreover, the equality of both peaks

could be purely coincidental and the surface may consist of a mixture of Li_2CO_3 and other species including carbon atoms in a one-oxygen environment, like oligomers of polyethylene oxide $(-CH_2CH_2O-)_n$ for example, since this kind of compounds could be identified on the same kind of samples without washing by acetonitrile [13]. Therefore, the sole analysis of C 1s core peaks is not sufficient to remove the indetermination. Quantification over all core peaks (not detailed here) showed that the main compounds of both surface layers are carbon-containing species, and that the other major constituent is LiF [27]. The analysis of valence spectra will be necessary to clearly identify all compounds.

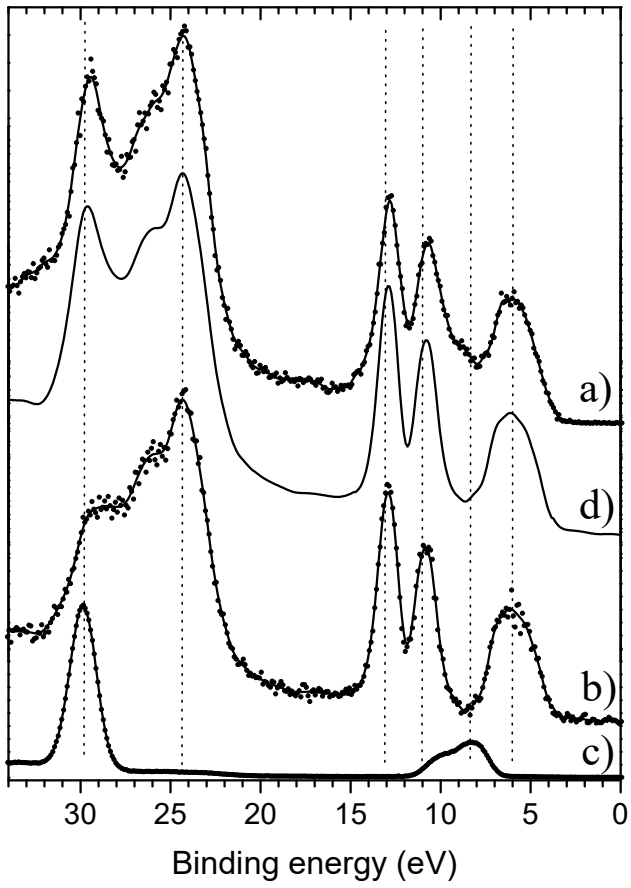

Figure 9 : Experimental valence spectra of : **a)** layer after the first discharge, **b)** Li_2CO_3, **c)** LiF, and **d)** simulation obtained from spectra b) and c).

Figure 9 shows the experimental valence spectra of : *a)* the sample obtained after the first discharge of the cell, *b)* Li_2CO_3, *c)* LiF, and *d)* a simulated spectrum obtained by linear combination of spectra b) and c). As we can see in the figure, the valence spectrum of sample a) is rather simple. We can clearly identify all characteristic peaks of Li_2CO_3, as well as a narrow peak at 29.6 eV due to F 2s states of LiF, and a shoulder at 8-9 eV due to F 2p states of LiF. The simulated spectrum d) is very close to the experimental spectrum a), which shows undoubtedly that the major components of this surface layer are Li_2CO_3 and LiF.

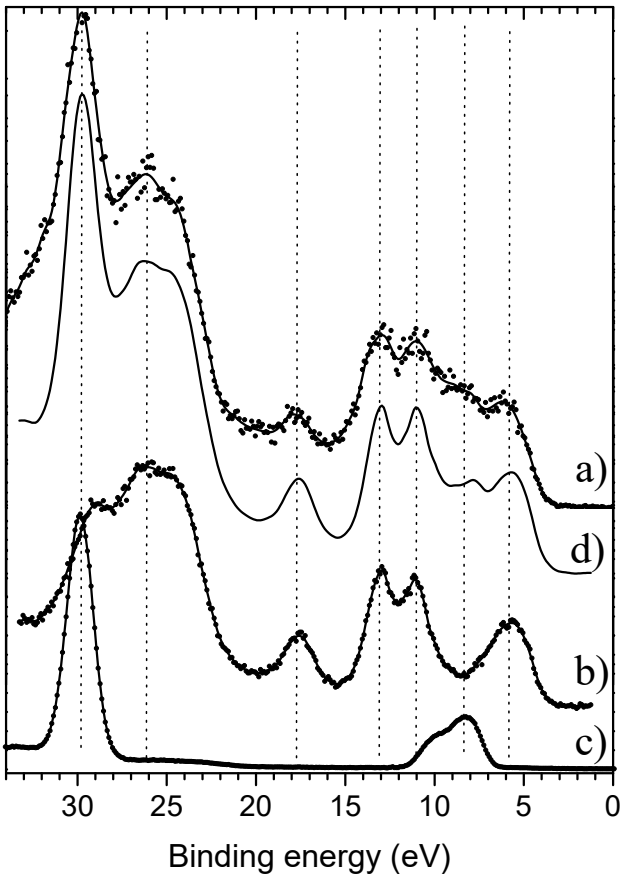

Figure 10 : Experimental valence spectra of : **a)** layer after 500 cycles, **b)** $MeOCO_2Li$, **c)** LiF, and **d)** simulation obtained from spectra b) and c).

Figure 10 shows the experimental valence spectra of : *a)* the sample obtained after 500 cycles of discharge/charge, *b)* $MeOCO_2Li$, *c)* LiF, and *d)* a simulated spectrum obtained from spectra b) and c). Once again, the spectrum of the electrode is rather simple. We can recognize the characteristic valence shape of $MeOCO_2Li$, which differs from that of Li_2CO_3 by the presence of an additional peak at 17.6 eV and by the decrease of the narrow peak at 24.3 eV, which is reduced to a simple shoulder. The characteristic peaks of LiF can be also identified by the presence of an intense narrow peak at 29.7 eV and a weak peak at 8-9 eV. The spectra of $MeOCO_2Li$ and LiF allow us to build a simulated spectrum d) that is very close to the experimental spectrum a), which shows undoubtedly that the major components of this surface layer are $MeOCO_2Li$ and LiF. Therefore, a careful analysis of the valence spectrum of this sample allows us to conclude that the Li alkyl carbonate that forms at the electrode/electrolyte interface is $MeOCO_2Li$ and not $EtOCO_2Li$ or $(-CH_2OCO_2)_2Li_2$. Moreover, this analysis associated to the observation of two peaks of equal intensity at 290.1 and 286.8 eV in the C 1s spectrum (fig. 8) allow us to affirm that the amount of Li_2CO_3 mixed to $MeOCO_2Li$ is very low in this sample. We can thus conclude that during electrochemical cycling of the cell, Li_2CO_3 and LiF form at the surface of the electrode upon the first discharge, and then that $MeOCO_2Li$ accumulates over the cycles.

CONCLUSION

In this study, we carried out the experimental XPS characterization of two Li alkyl carbonates : $MeOCO_2Li$ and $EtOCO_2Li$. By means of ab initio calculations, we could interpret and simulate satisfactorily their valence spectra. This way, we could simulate the

expected valence spectra of other Li alkyl carbonates, namely $PrOCO_2Li$, Li ethylene dicarbonate and Li propylene dicarbonate. We showed that a combined analysis of XPS core peaks and valence spectra allows to clearly identify the different Li alkyl carbonate species, and that this kind of analysis can be successfully used in the study of electrode/electrolyte interfaces. Taking as example the study of layers forming at the surface of stainless-steel cathodes in lithium cells, we applied the results of this approach and showed that the main Li alkyl carbonate species formed in this case was $MeOCO_2Li$.

REFERENCES

[1] Tarascon, J-M. ; Armand, M ; *Nature* **2001**, *414*, 359

[2] Wakihara, M. ; *Mater. Sci. Eng., R Rep.* **2001**, *R33*, 109-134

[3] Peled, E. ; *J. Electrochem. Soc.* **1979**, *126***,** 2047

[4] Peled, E.; Golodnitsky, D.; Ardel, G.; *J. Electrochem. Soc.* **1997**, *144*, L 208

[5] Nazri, G.; Muller, R. H.; *J. Electrochem. Soc.* **1985**, *132*, 2050

[6] Aurbach, D.; Daroux, M. L.; Faguy, P. W ; Yeager, E.; *J. Electrochem. Soc.* **1987**, *134*, 1611-1620

[7] Aurbach, D.; Ein-Eli, Y. ; Markovsky, B. ; Zaban, A. ; Luski, S. ; Carmeli, Y. ; Yamin, H. ; *J. Electrochem. Soc.* **1995**, *142*, 2882-2889

[8] Aurbach, D. ; Levi, M. D. ; Levi, E. ; Schechter, A. ; *J. Phys. Chem. B* **1997**, *101*, 2195-2206

[9] Gireaud, L. ; Grugeon, S. ; Laruelle, S. ; Pilard S. ; Tarascon, J-M. ; *J. Electrochem. Soc.* **2005**, *152*, A850-A857

[10] Poizot, P. ; Laruelle, S. ; Grugeon, S. ; Dupont, L. ; Tarascon, J-M. ; *Nature* **2000**, *407*, 496-499

[11] Grugeon , S. ; Laruelle , S. ; Herrera-Urbina, R. ; Dupont, L. ; Poizot , P. ; Tarascon, J-M. ; *J. Electrochem. Soc.* **2001**, *148*, A 285-292

[12] Dedryvère , R. ; Laruelle , S. ; Grugeon , S. ; Poizot , P. ; Gonbeau , D. ; Tarascon, J-M. ; *Chem. Mater.* **2004**, *16*, 1056-1061

[13] Laruelle, S. ; Pilard, S. ; Guenot, P. ; Grugeon, S. ; Tarascon, J-M. ; *J. Electrochem. Soc.* **2004**, *151*, A1202-A1209

[14] Pereira, N. ; Dupont, L. ; Tarascon, J-M. ; Klein, L. C. ; Amatucci, G. G. ; *J. Electrochem. Soc.* **2003**, *150*, A 1273

[15] Aurbach, D. ; Markovski, B. ; Weissmann, I. ; Levi, E. ; Ein-Eli, Y. ; *Electrochimica Acta* **1999**, *45*, 67-86

[16] Fong, R. ; Von Sacken, U. ; Dahn, J. R. ; *J. Electrochem. Soc.* **1990**, *137*, 2009

[17] Behrendt, W. ; Gattow, G. ; Dräger, M. ; *Z. anorg. allg. Chem.* **1973**, ***397***, 237-246

[18] Shirley, D. A. ; *Phys. Rev. B* **1972**, *5*, 4709

[19] Scofield, J. H. ; *J. Electron Spectrosc. Relat. Phenom.* **1976**, *8*, 129-137

[20] Gaussian 98, Revision A.11.3, M. J. Frisch, G. W. Trucks, H. B. Schlegel, G. E. Scuseria, M. A. Robb, J. R. Cheeseman, V. G. Zakrzewski, J. A. Montgomery, Jr., R. E. Stratmann, J. C. Burant, S. Dapprich, J. M. Millam, A. D. Daniels, K. N. Kudin, M. C. Strain, O. Farkas, J. Tomasi, V. Barone, M. Cossi, R. Cammi, B. Mennucci, C. Pomelli, C. Adamo, S. Clifford, J. Ochterski, G. A. Petersson, P. Y. Ayala, Q. Cui, K. Morokuma, N. Rega, P. Salvador, J. J. Dannenberg, D. K. Malick, A. D. Rabuck, K. Raghavachari, J. B. Foresman, J. Cioslowski, J. V. Ortiz, A. G. Baboul, B. B. Stefanov, G. Liu, A. Liashenko, P. Piskorz, I. Komaromi, R. Gomperts, R. L. Martin, D. J. Fox, T. Keith, M. A. Al-Laham, C. Y. Peng, A. Nanayakkara, M. Challacombe, P. M. W. Gill, B. Johnson, W. Chen, M. W. Wong, J. L. Andres, C. Gonzalez, M. Head-Gordon, E. S. Replogle, and J. A. Pople, Gaussian, Inc., Pittsburgh PA, 2002.

[21] Gelius, U.; "Electron spectroscopy", D. A. Shirley (ed.), North-Holland, Amsterdam, **1972**, 311

[22] Gelius, U.; *J. Electron Spectrosc. Relat. Phenom.* **1974**, *5*, 985

[23] Wyckoff, R. W. G. ; *"Crystal structures"*, vol. 2, 2nd ed. **1967**, Interscience Publishers, Wiley & Sons

[24] Matsuta, S. ; Asada, T. ; Kitaura, K. ; *J. Electrochem. Soc.* **2000**, *147*, 1695-1702

[25] Wang, Y. ; Balbuena, P. B. ; *J. Phys. Chem. A* **2002**, *106*, 9582-9594

[26] Pireaux, J. J. ; Svensson, S. ; Basilier, E. ; Malmqvist, P-Å. ; Gelius, U. ; Caudano, R. ; Siegbahn, K. ; *Phys. Rev. A* **1976**, *14*, 2133-2145

[27] Dedryvère, R. ; Laruelle, S. ; Grugeon, S. ; Gireaud, L. ; Tarascon, J-M. ; Gonbeau, D. ; *J. Electrochem. Soc.* **2005**, *152*, A689-A696